

Diffusion-based Iterative Counterfactual Explanations for Fetal Ultrasound Image Quality Assessment

Paraskevas Pegios^{1,4}, Manxi Lin¹, Nina Weng¹, Morten Bo Søndergaard Svendsen², Zahra Bashir³, Siavash Bigdeli¹, Anders Nymark Christensen¹, Martin Tolsgaard², and Aasa Feragen^{1,4}

¹ Technical University of Denmark, Kongens Lyngby, Denmark
{ppar,afhar}@dtu.dk

² Region Hovedstaden Hospital, Copenhagen, Denmark

³ Slagelse Hospital, Copenhagen, Denmark

⁴ Pioneer Centre for AI, Copenhagen, Denmark

Abstract. Obstetric ultrasound image quality is crucial for accurate diagnosis and monitoring of fetal health. However, producing high-quality standard planes is difficult, influenced by the sonographer’s expertise and factors like the maternal BMI or the fetus dynamics. In this work, we propose using diffusion-based counterfactual explainable AI to generate realistic high-quality standard planes from low-quality non-standard ones. Through quantitative and qualitative evaluation, we demonstrate the effectiveness of our method in producing plausible counterfactuals of increased quality. This shows future promise both for enhancing training of clinicians by providing visual feedback, as well as for improving image quality and, consequently, downstream diagnosis and monitoring.

Keywords: Explainable AI · Diffusion Models · Fetal Ultrasound

1 Introduction

The quality of obstetric ultrasound screening images is crucial for the clinical downstream tasks [32], involving fetal growth estimation, preterm birth predic-

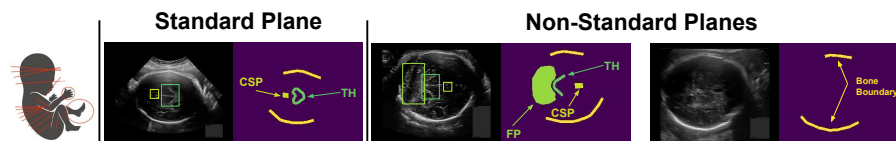


Fig. 1: Standard planes (SPs) are defined as particular anatomical planes through the body (left); here we show examples of high-quality SPs (middle) and low-quality non-standard planes (NSPs) (right) for the fetal head. A fetal head SP should show thalamus (TH), cavum septi pellucidum (CSP), but *not* fossa posterior (FP). The bone boundaries should support the correct placement of calipers.

tion, as well as abnormality detection. If the captured anatomical planes are not precise or the anatomical regions to be measured are not visualized well, then the measurements and estimated outcomes will be incorrect (Fig. 1). To standardize image quality, international ultrasound societies establish precise criteria for defining fetal ultrasound quality [28]. However, the acquisition of high-quality images is hampered both by the clinician’s level of training and by physical characteristics such as maternal BMI or the fetus’ position. As a result, acquiring *standard planes* of sufficiently high quality can be very challenging.

As a step towards solving this problem, we develop a method for generating *counterfactuals* that, taking a fetal ultrasound image as input, predicts how a *higher quality* image of the same anatomy would have looked like. This is motivated by potential future applications [21] in two rather different use cases: First, by showcasing a path from the acquired image to a higher-quality standard plane of the same anatomy, we can support less experienced clinicians in learning to acquire better ultrasound images. Second, if a non-standard plane ultrasound image can be used to generate a higher-quality standard plane of the same anatomy, this might be used to obtain better outcome predictions for those patients where high-quality standard planes are hard to acquire.

Our method builds on existing diffusion-based counterfactual explainable AI (XAI) methods from computer vision. However, these need further development to be useful for fetal ultrasound: Traditional counterfactual XAI methods are largely developed for images of faces [9,10,31], e.g. to generate smiling versions of famous people. As one’s identity should not change, and as these counterfactuals can often be obtained by changing only a few pixels, sparsity constraints [9,10] and masked inpainting [31] are often applied as data fidelity terms to leave one’s identity unchanged. For fetal ultrasound, however, improved image quality often requires changing *many* pixels: Blur typically occurs over large regions, and correcting an anatomically incorrect plane requires changing the entire image. To this end, we contribute a) an iterative counterfactual explanation approach that drives toward higher confidence counterfactuals achieving broad changes to the input and b) an extensive evaluation that demonstrates that we can produce plausible high-quality counterfactuals for fetal ultrasound images.

2 Related Work

Over recent years, deep learning methods have supported fetal ultrasound quality assessment, including image-based [13,14,32] and video-based [16,19,34] approaches. Other approaches focus on the generation of synthetic fetal ultrasound images [21] either to improve fine-grained classification [11,17,24] or to generate training material for novice sonographers [4,12,20]. The success of Denoising Diffusion Probabilistic Models [7,25] (DDPMs) enables the creation of highly realistic fetal ultrasound images [8] or the detection of out-of-distribution frames from fetal ultrasound videos [23]. Aligned with our motivation for supporting non-experts, [20] employs a GAN-based method with domain adaptation to predict a high-quality standard plane using previous video frames. In our work,

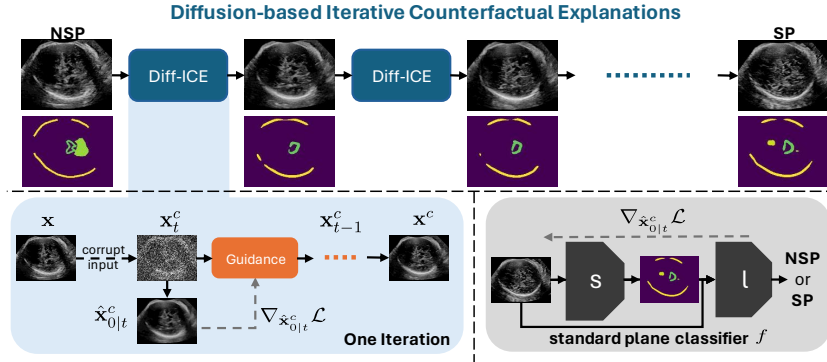


Fig. 2: **Top:** Each iteration uses previous output to enhance counterfactual confidence. **Bottom-left:** Efficient gradient estimation at each time step t for one iteration. **Bottom-right:** Standard plane classifier and guiding gradient flow.

we rely on image inputs and leverage diffusion-based counterfactual explanations to predict the path from low-quality to high-quality images.

Counterfactual explanations try to answer the question: How does an image look like if it is classified differently by a given classifier? Different from adversarial examples, counterfactuals should be realistic, i.e., close to the data manifold which is usually approximated with generative models. In medical imaging, different methods have been proposed including VAE-based [3], GAN-based [30] and diffusion-based [27, 29] approaches. Yet, these are applied to tasks where changes are highly localized. In our work, we leverage recent advancements in diffusion guidance [5] and counterfactuals [31] to apply a computationally feasible iterative approach where each step utilizes a perceptual loss as a data fidelity term, rather than sparsity [9, 10] or inpainting [10, 31] to refine diffusion-based counterfactuals. This allows us to achieve more global counterfactual changes.

3 Method

3.1 Preliminaries on Diffusion Models

DDPMs [7] are defined by two processes: The forward and the reverse. In the former, an input image \mathbf{x}_0 is gradually corrupted by adding Gaussian noise at each time step t , while the latter gradually removes it to generate a clean image. Formally, the forward process is defined by generating the time t image $\mathbf{x}_t \sim \mathcal{N}(\sqrt{1 - \beta_t} \mathbf{x}_{t-1}, \beta_t \mathbf{I})$ iteratively from the original, clean image \mathbf{x}_0 , where $\{\beta\}_{t=1:T}$ controls the variance of the noise added per step. The time t image \mathbf{x}_t can be sampled directly [25] using \mathbf{x}_0 and the reparametrization trick,

$$\mathbf{x}_t = \sqrt{\alpha_t} \mathbf{x}_0 + \epsilon \sqrt{1 - \alpha_t}, \epsilon \sim \mathcal{N}(0, 1), \quad (1)$$

where $\alpha_t = 1 - \beta_t$ and $\bar{\alpha}_t = \prod_{s=1}^t \alpha_s$. The reverse process also consists of Gaussian transitions whose mean and covariance are predicted by neural networks:

$\mathbf{x}_{t-1} \sim \mathcal{N}(\mu_\theta(\mathbf{x}_t, t), \Sigma_\theta(\mathbf{x}_t, t))$, where $\mathbf{x}_T \sim \mathcal{N}(\mathbf{0}, \mathbf{I})$. In practice, a denoiser $\epsilon_\theta(\mathbf{x}_t, t)$ predicts the noise from Eq. (1) rather than predicting the mean $\mu_\theta(\mathbf{x}_t, t)$ directly, giving $\mu_\theta(\mathbf{x}_t, t) = \frac{1}{\sqrt{1-\beta_t}} \left(\mathbf{x}_t - \frac{\beta_t}{\sqrt{1-\alpha_t}} \epsilon_\theta(\mathbf{x}_t, t) \right)$.

3.2 Diff-ICE: Diffusion-based Iterative Counterfactual Explanations

We quantify image quality using a classifier f , which is trained to predict whether fetal ultrasound images are standard or non-standard (SP or NSP) planes. As both ultrasound image quality [14] and outcome prediction [26] benefit from combining images with segmentations, classifier f consists of a segmentation model s and a predictor l trained sequentially. The classifier takes as inputs the image and the segmentation predictions, $f(\mathbf{x}) = l(s(\mathbf{x}), \mathbf{x})$. This adds explainability to the classifier, as the segmentations can be visualized as partial explanations.

Following [9, 31], we corrupt the input \mathbf{x} up to a limited noise level τ , with $1 \leq \tau \leq T$, using Eq.(1) to initialize a noisy version of the input and guide \mathbf{x}_τ^c towards the desired counterfactual class y with guided diffusion [4]. To this end, we minimize a loss function \mathcal{L} and shift the average sample with its gradient g ,

$$\mathbf{x}_{t-1}^c \sim \mathcal{N}(\mu_\theta(\mathbf{x}_t^c, t) - \Sigma_\theta(\mathbf{x}_t^c, t)g, \Sigma_\theta(\mathbf{x}_t^c, t)). \quad (2)$$

As the classifier f is trained on clean images, we use the learned denoiser to get one-step denoised predictions and pass them through f by solving Eq.(1) for \mathbf{x}_0 ,

$$\hat{\mathbf{x}}_{0|t}^c = \frac{\mathbf{x}_t^c - \sqrt{1 - \alpha_t} \epsilon_\theta(\mathbf{x}_t^c, t)}{\sqrt{\alpha_t}}, \quad (3)$$

Computing the gradient w.r.t. \mathbf{x}_t^c as in [1, 33], i.e. $g = \nabla_{\mathbf{x}_t^c} \mathcal{L}$, necessitates backpropagating through the denoiser. As this is computationally expensive, we instead follow an efficient gradient estimation [5, 31] which avoids excessive backpropagation and speeds up sampling. Thus, for each t , we compute gradients w.r.t $\hat{\mathbf{x}}_{0|t}^c$, i.e. $g = \nabla_{\hat{\mathbf{x}}_{0|t}^c} \mathcal{L}$ in Eq. (2). We use the counterfactual guiding loss

$$\mathcal{L}(\mathbf{x}, \hat{\mathbf{x}}_{0|t}^c, y) = \lambda_c \mathcal{L}_c \left(f \left(\hat{\mathbf{x}}_{0|t}^c \right), y \right) + \lambda_p \mathcal{L}_p \left(\hat{\mathbf{x}}_{0|t}^c, \mathbf{x} \right), \quad (4)$$

where \mathcal{L}_c is the classification loss which guides towards the desired label y , \mathcal{L}_p is an l2-based perceptual loss which guides the process in terms of proximity, and λ_c and λ_p are hyperparameters which control the guidance strength. Typical applications focus on localized counterfactual changes and use a pixel-based l1-norm for \mathcal{L}_p [10, 31] or this is added as an extra term on the noisy images [9]. Our loss function prioritizes broad changes while preserving anatomical fidelity.

Yet, achieving global changes is challenging, as setting τ for a limited noise level preserves semantic information in one-step denoised predictions but allows guidance mostly in refinement stages [33]. Increasing the strength of λ_c may result in not meaningful generations [1]. Thus, we propose a **Diffusion-based Iterative Counterfactual Explanation** approach (Diff-ICE) to enhance confidence in counterfactuals and enable more global alterations. Through L iterations of

the counterfactually guided reverse process, each using the previous output as input, we refine the counterfactuals while maintaining fidelity constraints close to the original input \mathbf{x} in Eq. (4). Our approach is summarized in Fig. 2.

4 Experiments and Results

Data and base implementation. We work with two datasets extracted from a national fetal ultrasound screening database (ANONYMIZED). The **GROWTH** dataset, which is used to train both the unconditional diffusion model and a segmentation model used in the guiding standard plane classifier f , consists of 4363 (2842/1521 for train/test) fetal ultrasound images from growth scans including head, abdomen, femur, and cervix images. The **HEAD** dataset is used to train and test the full guiding classifier f , and consists of fetal *head* ultrasound images which include 240 high-quality standard planes (SP) and 1339 low-quality non-standard planes (NSP).

As the guiding **standard plane classifier** f we choose a robust and interpretable architecture that combines a DTU-Net [15] segmentation model s with a SonoNet-16 [2] classifier l following [26]. Robustness is important to ensure high-quality counterfactuals, and interpretability makes the counterfactuals easier to monitor both for technical developers and clinicians at different levels of experience. The segmentation model s is developed on **GROWTH**. Thus, we train and evaluate the classifier’s predictor l sequentially keeping the weights of g fixed on a split of 121/26/93 SP and 712/204/423 NSP images for train/validation/test with non-overlapping patients resulting in 78% balanced test accuracy.

An **unconditional DDPM** [7] is also trained on **GROWTH** using 1000 diffusion steps, following model architecture described in [9], training for 300K iterations with batch size 16, learning rate 10^{-4} , weight decay of 0.05, and no dropout. For all models, images are resized to 224×288 , embedded text and calipers are removed [22] and pixel intensity is normalized to $[-1, 1]$.

To generate **counterfactual explanations**, we empirically set $L = 5$, $\tau = 120$ of 400 re-spaced time steps, $\lambda_p = 30$ and search for $\lambda_c \in \{40, 60, 80\}$ [9]. The perceptual loss uses a ResNet-50 trained on RadImageNet [18].

Baselines. 1) DiME [9] employs an expensive nested loop of the reverse guided processes per time step t to obtain clean images and applies a scaling trick to estimate gradients w.r.t. noisy images. 2) A single iteration of Diff-ICE, henceforth Diff-ICE₁, implements FastDiME [31] without mask-based inpainting (this is tailored for localized changes and would be a disadvantage in our setting). 3) Inspired by [1] we implement Diff-ICE_{1-x_t} taking the gradient w.r.t. noisy images. For fair comparison, baselines use the same loss (Eq. (4)) and hyperparameters.

Performance metrics. We evaluate *realism* by computing Fréchet Inception Distance [6] (FID) and Fréchet SonoNet Distance [12] (FSD) between the original NSP images and their valid SP counterfactuals. We further introduce SonoSim,

Table 1: Comparison of Diff-ICE with baseline diffusion-based approaches.

Method	Realism			Validity				Efficiency		
	FID ↓	FSD ↓	SonoSim ↑	MQD ↑	BKL ↓	MAD ↑	FR ↑	Batch Time (s)	Total Time (h)	GPU M (GB)
DiME	41.5	0.396	0.854	0.291	0.391	0.231	0.966	3151.9 ± 730.4	37.65	9.6
Diff-ICE _{1-x_t}	39.9	0.403	0.855	0.301	0.413	0.208	0.936	231.4 ± 56.8	2.77	33.7
Diff-ICE ₁	39.0	0.355	0.856	0.253	0.387	0.234	0.982	115.6 ± 34.2	1.38	9.6
Diff-ICE	42.4	0.435	0.790	0.371	0.336	0.284	0.982	448.6 ± 22.9	5.27	9.6

Table 2: Intermediate results for each iteration of Diff-ICE.

Iteration	Realism			Validity			Efficiency	
	FID ↓	FSD ↓	SonoSim ↑	MQD ↑	BKL ↓	MAD ↑	Batch Time (s)	Iteration Time (h)
1	38.96	0.355	0.856	0.253	0.387	0.234	115.6 ± 34.2	1.38
2	41.26	0.420	0.830	0.317	0.370	0.250	88.6 ± 22.3	1.06
3	42.25	0.464	0.818	0.314	0.362	0.258	85.8 ± 21.9	1.03
4	43.17	0.454	0.807	0.355	0.357	0.262	77.9 ± 18.7	0.96
5	42.42	0.435	0.790	0.371	0.336	0.284	78.9 ± 17.4	0.95

which computes the cosine similarity using SonoNet-64 [2] features, similar to those used in FSD. To measure *validity* of generated images, we use standard counterfactual validity metrics from computer vision such as Flip Ratio (FR), i.e., the frequency of counterfactuals classified as SP, Mean Absolute Difference [31] (MAD) of confidence prediction between original NSP and counterfactual SP, and Bounded remapping of KL divergence [9] (BKL), which measures similarity between the counterfactual’s prediction by f , and the SP one-hot counterfactual label. The validity metrics BKL, MAD, and FR are computed for those NSP test images that are classified as NSP by f . In addition to verifying that counterfactuals indeed move towards the SP class according to the guiding classifier f , we develop a Progressive Concept Bottleneck Model [14] (PCBM) as an *oracle* using **GROWTH**, and use its confidence to measure overall Quality Scores (QS_O) for both input \mathbf{x} and counterfactual \mathbf{x}^c . To simulate a realistic evaluation scenario and ensure reliable oracle predictions for our analysis, we include cases with confident predictions of the original NSP input, i.e., original inputs \mathbf{x} classified as NSP, $QS_O(\mathbf{x}) < 0.5$ (see Fig. S2 in Supplementary Material). As an *oracle validity* metric, we introduce Mean overall Quality Difference defined as $MQD = \frac{1}{N} \sum_{i=1}^N I(QS_O(\mathbf{x}_i) < 0.5) \cdot QD_O(\mathbf{x}_i^c, \mathbf{x}_i)$ where I is the indicator function, $N = 423$ NSP test images and $QD_O(\mathbf{x}^c, \mathbf{x}) = QS_O(\mathbf{x}^c) - QS_O(\mathbf{x})$. To evaluate *efficiency*, we compute batch time in seconds, total time in hours, and GPU memory, using a batch size of 10 on an NVIDIA RTX A6000.

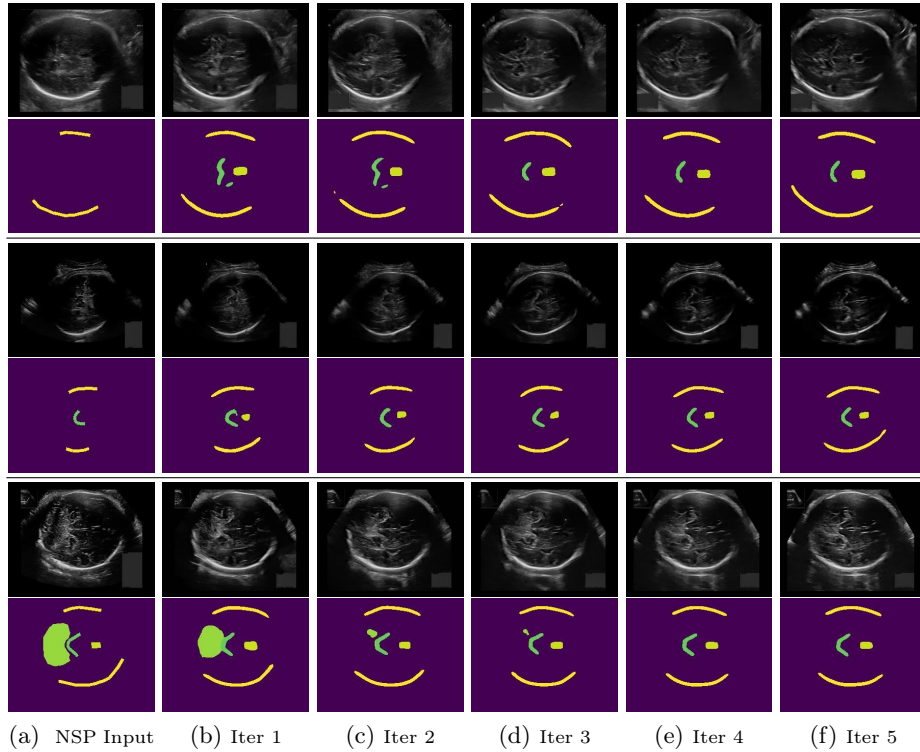


Fig. 3: Iterations of Diff-ICE from the low-quality NSP to a higher-quality SP, visualized with predicted segmentations for interpretability (expert mask annotation for NSP input). Diff-ICE can synthesize planes that (correctly) contain **thalamus (TH)**, and **cavum septi pellucidi (CSP)** from NSP planes that don't contain this. It is also capable of creating planes that (correctly) remove **fossa posterior (FP)**. In addition to these local and explicit changes, Diff-ICE also achieves broad changes and refinements.

Results. We generated counterfactual explanations for all 423 NSP test images from **HEAD**. Tables 1 and 2 list results for all methods and each intermediate iteration of Diff-ICE, respectively. Note that there is an expected inverse relationship between realism (similarity to input) and validity (improved SP prediction), meaning that the choice of iterations is a trade-off. Table 2 illustrates this trend, with realism decreasing as validity increases with more iterations. We chose $L = 5$ due to small qualitative differences between 4th and 5th iteration, as shown in Fig. 3, illustrating paths from low-quality NSP to higher-quality SP.

In addition to image-level SP confidence scores, the oracle PCBM [14] also predicts individual quality scores (QS_{FP} , QS_{CSP} and QS_{TH} for **fossa posterior (FP)**, **cavum septi pellucidi (CSP)**, and **thalamus (TH)**). As a fine-grained assess-

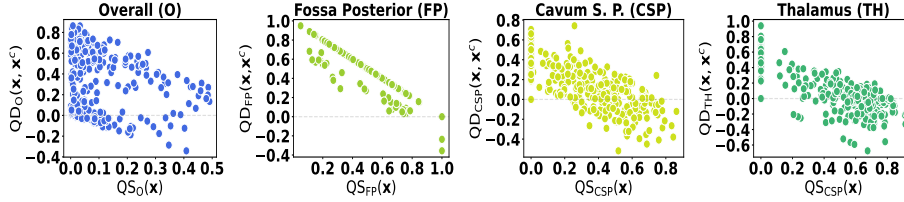


Fig. 4: Quality Difference (QD) as a function of NSP input’s Quality Score (QS).

ment of Diff-ICE, we show their quality score differences between counterfactual and NSP input (QD_{FP} , QD_{CSP} , QD_{TH}) as a function of input’s quality in Fig. 4.

Qualitative validation. A Fetal Medicine consultant with 10 years of experience in obstetric imaging was asked to select the best quality image from pairs of real NSP images and associated Diff-ICE counterfactuals. Image pairs with $QD_O > 0$ were sampled uniformly, and displayed in randomized position and order. The expert selected Diff-ICE counterfactuals in 41 out of 50 image pairs, demonstrating the ability of Diff-ICE to indeed enhance the input’s quality. The expert also stated qualitatively that differences were global, including improved presentation of bone outlines, **TH**, and **CSP**, and improved overall image quality.

Ablation study. We conducted an ablation study to assess the impact of parameters τ and λ_c , in our single iteration baseline Diff-ICE₁, relative to our iterative method Diff-ICE, as well as to investigate the influence of \mathcal{L}_p in Eq. 4. We observed that trying to achieve global counterfactual changes by increasing classifier’s strength too much ($\lambda_c = 400$) leads to adversarial examples while increasing the input noise level too much ($\tau = 200$) results in changes in the anatomy of the head or collapse to adversarial examples too. In all cases, removing the \mathcal{L}_p impacts the realism of counterfactuals. Detailed quantitative results (Tab. S3) and visual examples (Fig. S1) can be found in Supplementary Material.

5 Discussion and Conclusion

Our experimental results highlight the effectiveness of our iterative approach to produce higher confidence counterfactuals and broader changes compared to the single iteration baselines. Our method is computationally feasible, leveraging the efficient gradient estimation scheme we employ. From Fig. 4 we see that improvement is largest when the initial quality is poor, which is intuitive, as changes to already high-quality images should be minimal. For all three anatomical structures, the image quality associated with the structure is generally improved by the counterfactual. Diff-ICE performs particularly well in removing the unwanted **FP**, whereas there are some cases where, in particular, **TH** and **CSP** are

not improved. We note, however, that these cases feature fairly well-represented structures in the inputs and our method balances overall image-level quality with the quality of individual structures (see Fig. S3 in Supplementary Material).

To conclude, we propose Diff-ICE, to enhance confidence in counterfactuals and enable global changes. Our method demonstrates its capability to produce plausible counterfactual explanations for the challenging task of fetal ultrasound quality assessment as well as its potential for future applications.

Acknowledgements. This work was supported by the Pioneer Centre for AI (DNRF grant nr P1), the DIREC project EXPLAIN-ME (9142-00001B), and the Novo Nordisk Foundation through the Center for Basic Machine Learning Research in Life Science (NNF20OC0062606). P.P. would like to thank Thanos Delatolas for insightful discussions.

References

1. Bansal, A., Chu, H.M., Schwarzschild, A., Sengupta, S., Goldblum, M., Geiping, J., Goldstein, T.: Universal guidance for diffusion models. In: IEEE/CVF Conference on Computer Vision and Pattern Recognition. pp. 843–852 (2023)
2. Baumgartner, C.F., Kamnitsas, K., Matthew, J., Fletcher, T.P., Smith, S., Koch, L.M., Kainz, B., Rueckert, D.: Sononet: real-time detection and localisation of fetal standard scan planes in freehand ultrasound. *IEEE transactions on medical imaging* **36**(11), 2204–2215 (2017)
3. Cohen, J.P., Brooks, R., En, S., Zucker, E., Pareek, A., Lungren, M.P., Chaudhari, A.: Gifsplanation via latent shift: a simple autoencoder approach to counterfactual generation for chest x-rays. In: *Medical Imaging with Deep Learning*. PMLR (2021)
4. Dhariwal, P., Nichol, A.: Diffusion models beat gans on image synthesis. *Advances in neural information processing systems* **34**, 8780–8794 (2021)
5. He, Y., Murata, N., Lai, C.H., Takida, Y., Uesaka, T., Kim, D., Liao, W.H., Mitsu-fuji, Y., Kolter, J.Z., Salakhutdinov, R., et al.: Manifold preserving guided diffusion. In: *The Twelfth International Conference on Learning Representations* (2023)
6. Heusel, M., Ramsauer, H., Unterthiner, T., Nessler, B., Hochreiter, S.: Gans trained by a two time-scale update rule converge to a local nash equilibrium. *Advances in neural information processing systems* **30** (2017)
7. Ho, J., Jain, A., Abbeel, P.: Denoising diffusion probabilistic models. *Advances in neural information processing systems* **33**, 6840–6851 (2020)
8. Iskandar, M., Mannering, H., Sun, Z., Matthew, J., Kerdegari, H., Peralta, L., Xochicale, M.: Towards realistic ultrasound fetal brain imaging synthesis. In: *Medical Imaging with Deep Learning, short paper track* (2023)
9. Jeanneret, G., Simon, L., Jurie, F.: Diffusion models for counterfactual explanations. In: *Asian Conference on Computer Vision*. pp. 858–876 (2022)
10. Jeanneret, G., Simon, L., Jurie, F.: Adversarial counterfactual visual explanations. In: *IEEE/CVF Conference on Computer Vision and Pattern Recognition* (2023)
11. Lasala, A., Fiorentino, M.C., Micera, S., Bandini, A., Moccia, S.: Exploiting class activation mappings as prior to generate fetal brain ultrasound images with gans. In: *2023 45th Annual International Conference of the IEEE Engineering in Medicine & Biology Society (EMBC)*. pp. 1–4. IEEE (2023)

12. Lee, L.H., Noble, J.A.: Generating controllable ultrasound images of the fetal head. In: 17th International Symposium on Biomedical Imaging (ISBI). pp. 1761–1764. IEEE (2020)
13. Lin, M., Ambsdorf, J., Sejer, E.P.F., Bashir, Z., Wong, C.K., Pegios, P., Raheli, A., Svendsen, M.B.S., Nielsen, M., Tolsgaard, M.G., et al.: Learning semantic image quality for fetal ultrasound from noisy ranking annotation. arXiv preprint arXiv:2402.08294 (2024)
14. Lin, M., Feragen, A., Bashir, Z., Tolsgaard, M.G., Christensen, A.N.: I saw, i conceived, i concluded: Progressive concepts as bottlenecks. arXiv:2211.10630 (2022)
15. Lin, M., Zepf, K., Christensen, A.N., Bashir, Z., Svendsen, M.B.S., Tolsgaard, M., Feragen, A.: Dtu-net: Learning topological similarity for curvilinear structure segmentation. In: International Conference on Information Processing in Medical Imaging. pp. 654–666. Springer (2023)
16. Liu, S., Ying, Q., He, S., Yang, X., Ni, D., Huang, R.: Hierarchical agent-based reinforcement learning framework for automated quality assessment of fetal ultrasound video. In: 20th International Symposium on Biomedical Imaging (ISBI). pp. 1–5. IEEE (2023)
17. Maack, L., Holstein, L., Schlaefer, A.: Gans for generation of synthetic ultrasound images from small datasets. *Current Directions in Biomedical Engineering* **8**(1), 17–20 (2022)
18. Mei, X., et al.: Radimagenet: an open radiologic deep learning research dataset for effective transfer learning. *Radiology: Artificial Intelligence* **4**(5), e210315 (2022)
19. Men, Q., Teng, C., Drukker, L., Papageorghiou, A.T., Noble, J.A.: Multimodal-guidenet: Gaze-probe bidirectional guidance in obstetric ultrasound scanning. In: International Conference on Medical Image Computing and Computer-Assisted Intervention. pp. 94–103. Springer (2022)
20. Men, Q., Zhao, H., Drukker, L., Papageorghiou, A.T., Noble, J.A.: Towards standard plane prediction of fetal head ultrasound with domain adaption. In: 20th International Symposium on Biomedical Imaging (ISBI). pp. 1–5. IEEE (2023)
21. Mendez, M., Sundararaman, S., Probyn, L., Tyrrell, P.N.: Approaches and limitations of machine learning for synthetic ultrasound generation: A scoping review. *Journal of Ultrasound in Medicine* **42**(12), 2695–2706 (2023)
22. Mikolaj, K., Lin, M., Bashir, Z., Svendsen, M.B.S., Tolsgaard, M., Nymark, A., Feragen, A.: Removing confounding information from fetal ultrasound images. arXiv:2303.13918 (2023)
23. Mishra, D., Zhao, H., Saha, P., Papageorghiou, A.T., Noble, J.A.: Dual conditioned diffusion models for out-of-distribution detection: Application to fetal ultrasound videos. In: International Conference on Medical Image Computing and Computer-Assisted Intervention. pp. 216–226. Springer (2023)
24. Montero, A., Bonet-Carne, E., Burgos-Artizzu, X.P.: Generative adversarial networks to improve fetal brain fine-grained plane classification. *Sensors* **21** (2021)
25. Nichol, A.Q., Dhariwal, P.: Improved denoising diffusion probabilistic models. In: International Conference on Machine Learning. pp. 8162–8171. PMLR (2021)
26. Pegios, P., Sejer, E.P.F., Lin, M., Bashir, Z., Svendsen, M.B.S., Nielsen, M., Petersen, E., Christensen, A.N., Tolsgaard, M., Feragen, A.: Leveraging shape and spatial information for spontaneous preterm birth prediction. In: International Workshop on Advances in Simplifying Medical Ultrasound. pp. 57–67. Springer (2023)
27. Ribeiro, F.D.S., Xia, T., Monteiro, M., Pawlowski, N., Glocker, B.: High fidelity image counterfactuals with probabilistic causal models. In: International Conference on Machine Learning. pp. 7390–7425. PMLR (2023)

28. Salomon, L., et al.: Isuog practice guidelines: ultrasound assessment of fetal biometry and growth. *Ultrasound in obstetrics & gynecology* **53**(6), 715–723 (2019)
29. Sanchez, P., Kascenas, A., Liu, X., O’Neil, A.Q., Tsaftaris, S.A.: What is healthy? generative counterfactual diffusion for lesion localization. In: *MICCAI Workshop on Deep Generative Models*. pp. 34–44. Springer (2022)
30. Singla, S., Eslami, M., Pollack, B., Wallace, S., Batmanghelich, K.: Explaining the black-box smoothly—a counterfactual approach. *Medical Image Analysis* **84**, 102721 (2023)
31. Weng, N., Pegios, P., Feragen, A., Petersen, E., Bigdeli, S.: Fast diffusion-based counterfactuals for shortcut removal and generation. *arXiv preprint arXiv:2312.14223* (2023)
32. Wu, L., Cheng, J.Z., Li, S., Lei, B., Wang, T., Ni, D.: Fuiqa: fetal ultrasound image quality assessment with deep convolutional networks. *IEEE transactions on cybernetics* **47**(5), 1336–1349 (2017)
33. Yu, J., Wang, Y., Zhao, C., Ghanem, B., Zhang, J.: Freedom: Training-free energy-guided conditional diffusion model. In: *IEEE/CVF International Conference on Computer Vision*. pp. 23174–23184 (2023)
34. Zhao, H., Zheng, Q., Teng, C., Yasrab, R., Drukker, L., Papageorghiou, A.T., Noble, J.A.: Memory-based unsupervised video clinical quality assessment with multi-modality data in fetal ultrasound. *Medical Image Analysis* **90**, 102977 (2023)

Supplementary Material



Fig. S1: **Ablation study.** $\lambda_c = 400$ (c) results in not meaningful counterfactuals or adversarial noises. $\tau = 80$ (b) cannot achieve strong changes, and $\tau = 200$ (d) can lead to changes in the anatomy or collapse to adversarial examples.

Table S3: **Ablation study** on parameters τ , λ_c and the effect of \mathcal{L}_p .

Parameters		Realism			Validity			Efficiency	
τ	\mathcal{L}_p	FID ↓	FSD ↓	SonoSim ↑	MQD ↑	BKL ↓	MAD ↑	Batch Time (s)	Total Time (h)
80	✓	38.02	0.332	0.888	0.207	0.416	0.173	76.4±22.2	0.93
	✗	39.19	0.371	0.883	0.209	0.416	0.205	70.1±19.7	0.84
120	✓	38.96	0.355	0.856	0.253	0.387	0.234	115.6±34.2	1.38
	✗	40.66	0.427	0.851	0.259	0.388	0.234	88.5±25.2	1.06
	✓/ $\lambda_c = 400$	73.18	14.80	0.656	0.352	0.026	0.059	68.5±5.1	0.88
160	✓	41.30	0.417	0.827	0.303	0.367	0.255	131.9±39.9	1.61
	✗	42.04	0.482	0.821	0.332	0.368	0.253	108.3±31.2	1.30
200	✓	44.14	0.471	0.777	0.375	0.349	0.272	173.4±52.4	2.12
	✗	45.53	0.509	0.782	0.397	0.350	0.271	138.4±40.3	1.66

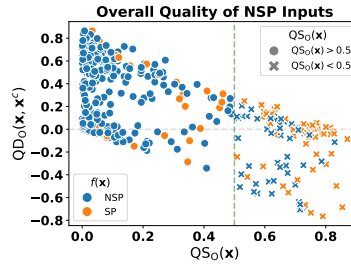


Fig. S2: **Oracle validity metric.** Quality Difference (QD) as a function of NSP input’s Quality Score (QS). The plot includes 417 valid Diff-ICE counterfactuals out of the 423 NSP inputs from our test set. To compute MQD we include 310 SP counterfactuals (circles) for which their original NSP is correctly predicted to have low image quality, i.e., $QS_O(\mathbf{x}) < 0.5$. The classifier f used for counterfactual guidance correctly predicts 330 (blue samples) of the NSP inputs.

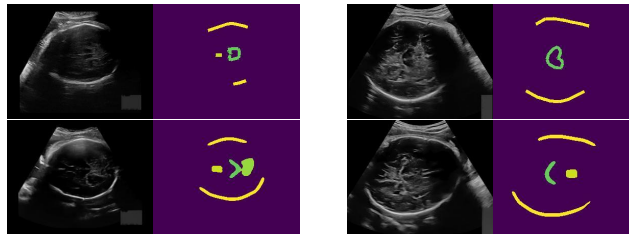


Fig. S3: **Limitations.** Rows: NSP inputs with segmentation annotations and Diff-ICE counterfactuals with segmentation predictions. Cases where expert chose NSP input: Diff-ICE balances quality by increasing overall and CSP quality but with the cost of slightly reducing TH (right) or FP (left) quality.